Application of DFNSIM to Teapot Dome

Eric B. Niven and Clayton V. Deutsch

This paper presents the use of the computer code, DFNSIM, for modelling the Tensleep Formation at Teapot Dome, which is a naturally fractured reservoir. The log, core and FMI data are examined in detail. The procedure for establishing relationships between core porosity and permeability are presented. FMI data is used to establish distributions of fracture properties such as intensity, aperture, size, local orientation and spacing. Available well picks are used to map horizons. Variograms are modelled and sequential Gaussian simulation is used to simulate rock matrix properties. Small-scale DFNs are simulated to model fractures at the well bore scale. The DFNs are shown to match target histograms of local fracture spacing and orientation as well as honoring the measured fracture intensity and number of intersections. The DFNs are upscaled to an equivalent permeability tensor and fracture porosity. The upscaled equivalent fracture permeability and porosity are used as data to inform area-wide sequential Gaussian simulation of fracture permeability and porosity.

Introduction

Research shows as much as 60% of the world's petroleum reserves are in naturally fractured reservoirs (NFRs) (Waldren and Corrigan, 1985; Beydoun, 1998 and Roxar, 2009) where the fractures in the reservoir rock have, or are predicted to have, a significant effect on the reservoir fluid flow. Previous studies by the authors have resulted in the development of a methodology and computer code that simulate discrete fracture networks (DFNs) that are more geologically realistic than those generated by existing codes (Niven and Deutsch, 2010a and Niven and Deutsch, 2010b). DFNSIM works by simulating more fractures than are required and optimizing to find a subset that best match input histograms of local fracture spacing, orientation, length, intensity and the number of fracture intersections.

The primary objective of this case study is to use the DFNSIM computer code to create a geologically realistic geological model of the Tensleep Formation, which is a known naturally fractured reservoir.

Background on Teapot Dome

Teapot Dome is located in Natrona County, Wyoming, about 30 miles north of Casper (Figure 1). Full-scale development of the field began in 1976 and production peaked in 1981. In 1992, the US Department of Energy created the Rocky Mountain Oilfield Testing Center (RMOTC) to manage the Teapot Dome field and converted it into a working laboratory. The RMOTC has collected a large amount of reservoir data and made it available to the public as non-proprietary data.

Hydrocarbons were produced from nine zones at Teapot Dome. The geologic column provided by the RMOTC is shown in Figure 2. The Tensleep Formation is the focus of this study. Production in the Tensleep is from the A and B Sandstones, which are separated by the Dolomite B unit. The B Sandstone is underlain by the C1 Dolomite. The Tensleep sandstone has a porosity of approximately 7% and is comprised of eolian dunes.

Three types of data are used in this study: core, geophysical logs and formation micro-images (FMI). The area of interest shown is 9000 feet wide by 15000 feet long (2.7 by 4.5 km) and is ideal since it includes three of five wells with FMI data but is a reasonable size for modelling. There are 29 wells with geophysical data and horizon picks located in the study area.

Exploratory Data Analysis

The geophysical log data is processed and extracted within each stratigraphic unit. Figure 3 shows histograms for porosity, water saturation and oil saturation in each of the three stratigraphic units. Porosity increases from 5% in the A Sandstone to 6% in the B Dolomite to 9% in the B Sandstone.

The available core data is used to calculate the bivariate relationships between porosity and horizontal permeability (k_h) and between porosity and vertical permeability (k_v) (See Figure 4) using the GSLIB program, BIMODEl (Deutsch and Dose, 2005). The conditional cumulative distribution functions

(CCDFs) are color coded from low (blue) to high (red) using the standard GSLIB color scale between the limits of 0 and 1. Values less than 0.01 or greater than 0.99 are not shown. The conditional mean values are connected by a solid black line, the 0.25 and 0.75 quantiles are shown by dashed black lines and the 0.05 and 0.95 quantiles are shown by the shorter dashed lines. The conditional mean line would normally fall in the middle, but the permeability CCDFs are skewed. These relationships between porosity and permeability are used later, along with simulations of porosity, to generate rock matrix models of horizontal and vertical permeability using a cloud transform (Deutsch and Does, 2005).

As noted earlier, FMI logs are available for five wells. The logs were interpreted by Randy Koepsell from Schlumberger. Koepsell compiled and interpreted the FMI data to provide estimates of fracture orientation and effective hydraulic fracture aperture in addition to classifying fractures as open, partially healed and induced (Koepsell, 2001, 2002a, 2002b, 2002c and 2004).

Figure 5 shows a stereonet with all available fracture poles from within the Tensleep Formation. The contoured steronet is also shown in the figure. Based on visual inspection of the contoured stereonet, the fractures is modeled as a single joint set. The mean pole trend and plunge are 7 degrees clockwise from north and 10 degrees from the horizontal plane, respectively.

Effective hydraulic aperture data is also available from the FMI logs. Figure 6 shows the average fracture aperture by geological unit. Apertures are the lowest in the tight B Dolomite and are highest in the Lower B Sandstone. Figure 7 shows relative frequency histograms of the natural logarithm of aperture. Also plotted on the charts are the normal distribution calculated using the mean and standard deviation of the Ln(aperture) data. The fit between the histograms and the normal distributions of Ln(aperture) appears reasonable, based on visual inspection, indicating that the aperture data is distributed approximately lognormally.

Fracture intensity is be defined by the dimension of the measurement region and the dimension of the fracture (Dershowitz and Herda, 1992). Common measures of fracture intensity include:

- a simple fracture count;
- P_{10}, the number of fractures per unit length (of borehole or scanline);
- P_{21}, fracture length per area (i.e. length of fractures on an outcrop);
- P_{32}, fracture area per volume.

The P_{10} fracture intensity is the easiest to measure in borehole FMIs while the P_{32} fracture intensity is used to simulate three-dimensional DFNs.

The FMI data is loaded into FracMan in order to calculate the P_{10} fracture intensity. `FracMan` also calculates an equivalent P_{32} fracture intensity from the P_{10} intensity through Monte Carlo simulation. This functionality is based on the work by Wang (2005) on stereological relationships between fracture orientation and fracture intensity. Table 1 shows the number of fractures per unit and borehole as well as the P_{10} and P_{32} fracture intensities. As is shown in the table, the middle B Dolomite unit shows the highest fracture intensity. This would make sense if the dolomite is more brittle than the sandstone units which over and underlay it.

The Teapot Dome dataset includes data on trace length measured from the FMIs. It is possible to estimate the fracture size distribution from the trace length distribution. This is made possible when not all fractures are imaged all the way around the borehole (this means that the fracture trace is a partial sinusoid rather than a full one). The ratio between the length of the partial fracture trace and the full sinusoid that would have been measured if the fracture fully intersected the borehole is called the trace length ratio. The trace length ratio is a function of the fracture orientation distribution, well geometry (borehole diameter and orientation) and the fracture size distribution. The distribution of fracture length can be estimated through simulation with different size distributions. The estimate of the fracture size distribution is non-unique, but often narrowly bounded (Golder Associates, 2010).

`FracMan` (Golder Associates, 2010) automates the calculation of the fracture size distribution from trace length data. There are some assumptions that must be made:

- All discontinuities are planar. This assumption is common in practice. At any rate, fracture curvature is often negligible (Warburton, 1980).
- Fractures are elliptical in shape and all fractures have the same aspect ratio, *k*.

- The fracture centroids are distributed randomly and independently in space (i.e. by a Poisson distribution).
- The fracture size is independent of their spatial location.

Zhang, Einstein and Dershowitz (2002) provide a lengthy discussion on each of these assumptions and they are deemed reasonable in most cases. FracMan calculates the mean and standard deviation of trace length and converts them to the mean and standard deviation of fracture radius for a few different distributions (see Table 2). For the Tensleep trace length data, the lognormal distribution is a better fit than the power law distribution or any of the other distributions. The mean and standard deviation of the lognormal fracture radius distribution are 19.4 and 12.9 feet, respectively. This analysis assumes circular fractures whereas DFNSIM simulates rectangular fractures. Making this assumption in order to calculate fracture size is considered reasonable given that aperture is much more important to fracture permeability than lateral fracture size and there is no other way to arrive at an appropriate fracture size distribution without outcrop data.

In addition to using DFNSIM to create DFNs, it can also be used to build the target histograms of local fracture spacing and orientation. The fractures that are indicated on the FMIs can be input into DFNSIM and the program will build the histograms of local fracture spacing and orientation (see Niven and Deutsch (2010) for more information on how these distributions are calculated). These two histograms are calculated for each of the five wells and are used as target distributions when simulating the DFNs in a later step.

Evaluating the target number of fracture intersections is difficult since we don't know the lateral extents of the fractures identified on FMIs. Although the centroid locations for fractures measured on FMIs are not known, they are assumed to be located vertically along the borehole trajectory. Fracture orientation is known from the FMI data. Fracture length is simulated from the lognormal distribution of fracture radius calculated earlier. DFNSIM checks every fracture to see if it intersects any other fractures to arrive at a total number of fracture intersections.

Horizon Mapping

Horizon picks are available in 29 wells in the area of interest. The horizons are mapped using the well picks as data. Simple global kriging (Neufeld and Wilde, 2005) is used to create maps of the horizon elevations that are free of data search artifacts. The calculated horizons are shown in Figure 9. In order to create artifact-free maps, all of the samples are used to calculate estimates at all locations. An omni-directional variogram with a long range of 10,000 feet (approximately 3 km) is used, which results in suitably smooth maps.

Between each of the four mapped horizons, isopachs are calculated (not shown). The average thickness of the A Sandstone, B Dolomite and B Sandstone units are 25 feet, 22 feet and 60 feet, respectively.

Stratigraphic Coordinates

Reservoir units are defined to provide a large-scale subdivision of the reservoir into geologically homogeneous units. Each unit is defined by a top and base surface grid. The surface grids are not flat due to differential compaction, structural deformation, erosion or subsequent deposition filling existing topography. As a result, the continuity of the facies and reservoir properties may not follow a convenient model grid definition.

One solution is to model the facies and reservoir properties in a transformed coordinate space. In this case, the strata conform to the existing top and base surfaces so vertical proportional coordinates are calculated and used in place of depth or elevation. Vertical proportional coordinates are the relative distance between a correlation top surface and base surface and are calculated as follows:

$$z_{rel} = \frac{z - z_{cb}}{z_{ct} - z_{cb}} T \tag{1}$$

Where:

- z_{rel} is 0 at the stratigraphic base surface and T at the stratigraphic top;

- T is a thickness constant equal to the average thickness of the unit;
- z_{cb} is the correlation base and z_{ct} is the correlation top.

Converting all depth measurements to proportional coordinates allows modelling of each reservoir layer in regular Cartesian coordinates. For this study, a vertical proportional coordinate is calculated for each geophysical log data within each of the three reservoir units.

Rock Matrix Modelling

All subsequent analysis and rock matrix modelling occurs in the depositional space defined by the proportional stratigraphic coordinates. The log data is declustered and then transformed to Gaussian space.

Variograms are calculated on the normal scores of porosity, water saturation and oil saturation within each of the three reservoir units. Figure 10 shows the experimental variograms and their fitted models for the A Sandstone (only the A Sandstone variograms are shown to save space). All variograms are fitted with spherical models with zero nugget effect. There is no anisotropy in the horizontal plane.

The rock properties are simulated using sequential Gaussian simulation (Deutsch and Journel, 1992). Each variable is simulated separately within each of the three reservoir units. The rock properties are simulated on a 30 x 50 x 25 cell grid in the x, y and z directions, respectively. The grid cells are 300 feet in the x and y directions and 1 foot in the z (vertical) direction. The simulated results are back-transformed to the original unit space. Figure 11 shows two cross sections through each the simulated models for A Sandstone porosity, water saturation and oil saturation.

Matrix permeability is modelled using `cltrans`, which uses a cloud transform of the simulated models of porosity and the conditional distributions shown in Figure 4. Figure 12 shows cross sections through a realization of horizontal and vertical permeability in the A Sandstone. The realizations of permeability are less continuous than the porosity realizations due to the cloud transform technique.

Fracture Modelling

The area of interest is 9,000 feet by 15,000 feet (2.7 km by 4.5 km). The average P_{32} fracture intensity in the 22 ft thick middle B Dolomite unit is 10.1 m^2/m^3. The grid volume is $3.0x10^9$ ft^3. If the average fracture is a square with the dimensions 20 by 20 feet, this means that the P_{32} intensity of one fracture is $1.3x10^{-7}$ m^2/m^3. If the target intensity is 10.1 m^2/m^3, this means that we need 74 million fractures to achieve the desired target intensity over the entire area of interest. It would take a number of days to calculate an optimized DFN of this size. Thus, instead of simulating a full field-size DFN, well bore scale DFNs are calculated at the location of the five wells with FMI data.

`DFNSIM` is used to calculate the optimized well bore scale DFNs. The DFNs are simulated in a region of 15 m in the x and y-directions and the thickness of the unit in the z-direction. Fractures are simulated using the input distributions of orientation, size and aperture identified by the exploratory data analysis. The DFNs are optimized so that the final DFNs closely match the target distributions of local fracture spacing and orientation, intensity and the number of intersections. Figure 13 shows the target, initial DFN and final DFN histograms of local fracture spacing and local fracture orientation for well 25-1-X-14 in the A Sandstone. The target and final histograms are near perfect matches. Moreover, the final P_{32} fracture intensity matches the target by within 2.3% and the final number of intersections is within 3.5% of the target number. Figure 14 shows an example of a DFN for well 25-1-X-14 in the A Sandstone.

DFN Upscaling

Most current approaches for flow simulation of NFRs rely on either the continuum or the DFN approach. Under the DFN approach, flow is simulated directly on the DFN fractures allowing incorporation of many of the characteristics of real fracture systems. Although the DFN approach can handle complex fracture geometry, its use has typically been limited to basic flow calculations and assumes zero permeability matrix rock. The continuum approach has seen far more use in actual practice. Under the continuum approach, the flow on a fracture is not directly simulated. Instead, the field is represented by grid blocks and an equivalent permeability is calculated for each one. The continuum approach has the advantage

that it can simulate complex recovery mechanisms such as capillary pressure and matrix-fracture interactions.

One of the most popular methods for calculating an equivalent permeability tensor is that of Oda (1985). Oda's approach has the advantage that it is fast and does not require flow simulation and can obtain effective properties for grid cells based directly on the geometry and properties of the fractures within those cells. However it does not take fracture connectivity into account and is limited to well-connected fracture networks.

Oda's approach lays a specified grid on top of a DFN and derives effective properties based on the fractures contained in each cell. The permeability tensor is:

$$k_{ij} = \frac{1}{12}\left(P_{kk}\delta_{ij} - P_{ij}\right) \tag{2}$$

Where:

- δ_{ij} is the Kroenecker delta
- $P_{kk} = P_{11} + P_{22}$
- $P_{ij} = \frac{1}{V}\sum_{k=1}^{N} l^2 e^3 n_{ik} n_{jk}$
- V is the grid cell volume
- l is the length of the fracture
- e is the fracture aperture
- n_{ik} and n_{jk} are the components of a unit normal to the fracture k

The reader is referred to Oda's paper and Niven and Deutsch (2009) for more details on the actual fracture permeability upscaling process.

Equivalent fracture permeability tensors (Kxx, Kyy and Kzz) and fracture porosity are calculated for the well bore scale DFNs. These well bore scale equivalent permeability tensors are used as data in the next step to inform field-wide fracture permeability and porosity simulations.

The DFNs are simulated in original coordinate space because the transform to proportional coordinate space would require an awkward transform of the fracture orientation distribution. However, the upscaled equivalent fracture porosity and permeability tensor can be easily transformed to proportional coordinates. Modelling of the fracture properties can now take place in the same proportional coordinate space as the rock matrix properties. Both models are simulated on the same grid definition allowing them to easily feed into a flow simulator.

Field Wide Fracture Permeability and Porosity Simulation

The equivalent permeability and porosity data are transformed to Gaussian space. Normal score semivariograms are calculated in the vertical direction. The vertical variograms for Kxx, Kyy, Kzz and fracture porosity are shown in Figure 15 for the A Sandstone. The variograms for the other two units are similar. The horizontal variograms are inaccessible since there are only five wells with fracture information. Thus, a horizontal to vertical anisotropy ratio of 100:1 is assumed. Deutsch (2002) indicates that ratios between 50:1 and 250:1 are reasonable.

Each of the three geological units are simulated separately. The sequential Gaussian simulations of the four fracture parameters each use their respective modelled variograms. The simulations are back transformed to original unit space. One realization of each of the four fracture variables for the A Sandstone is shown in Figure 16. Fracture porosity is quite small since the fractures themselves have very small apertures.

Conclusions

This paper presents an application of the DFNSIM computer code to modelling a real-world naturally fractured reservoir. This case study on the Tensleep Formation shows that DFNSIM can be used to generate geologically realistic models of reservoir fractures at the well bore scale. Along with the rock

matrix property models, the simulated models of fracture porosity and permeability can be input into a dual porosity flow simulator for further analysis.

References

Beydoun, Z.R., 1998, Arabian plate oil and gas; why so rich and so prolific? Episodes, Vol. 21, No. 3, 74-81.

Deutsch, C.V. and Dose, T., 2005, Programs for Debiasing and Cloud Tranformation: `bimodal` and `cltrans`, Annual Report 7, Centre for Computational Geostatistics, University of Alberta.

Dershowitz, W.S. and Herda, H.H., 1992, Interpretation of fracture spacing and intensity, 33rd US Symposium on Rock Mechanics, Santa Fe, NM, 757-766.

Deutsch, C.V., 2002, Geostatistical Reservoir Modeling, Oxford University Press, New York, 376pp.

Deutsch, C.V. and Journel, A.G., 1998, *GSLIB: Geostatistical Software Library and User's Guide*, Oxford University Press, New York, 2nd Ed., 369 pp.

Golder Associates, 2010, FracMan 7:Interactive discrete feature, data analysis, geometric modeling and exploration simulation. Golder Associates.

Koepsell, R., 2001, Fracture Analysis of FMI log for well 61-2-X-15 for the Department of Energy, Schlumberger-Oil Field Services.

Koepsell, R., 2002a, Fracture Analysis of FMI log for well 25-1-X-14 for the Department of Energy, Schlumberger-Oil Field Services.

Koepsell, R., 2002b, Fracture Analysis of FMI log for well 67-1-X-10 for the Department of Energy, Schlumberger-Oil Field Services.

Koepsell, R., 2002c, Fracture Analysis of FMI log for well 71-1-X-4 for the Department of Energy, Schlumberger-Oil Field Services.

Koepsell, R., 2004, Fracture Analysis of FMI log for well 48-X-28 for the Department of Energy, Schlumberger-Oil Field Services.

Neufeld, C. and Wilde, B., 2005, A Global Kriging Program for Artifact-Free Maps, Annual Report 7, Centre for Computational Geostatistics, University of Alberta.

Niven, E.B. and Deutsch, C.V., 2009, A sensitivity analysis for equivalent permeability tensors calculated from 2D discrete fracture networks, Annual Report 11, Centre for Computational Geostatistics, University of Alberta.

Niven, E.B. and Deutsch, C.V., 2010a, A new approach to DFN simulation, Annual Report 12, Centre for Computational Geostatistics, University of Alberta.

Niven, E.B. and Deutsch, C.V., 2010b, `DFNSIM`: A New Program for Simulating Discrete Fracture Networks, Annual Report 12, Centre for Computational Geostatistics, University of Alberta.

Oda, M., 1985, Permeability tensor for discontinuous rock masses, Geotechnique, Vol. 35, No. 4, 483-495.

Roxar, 2009, Naturally fractured reservoirs: an introduction to their appraisal and management [online]. Available from http://www.roxar.com/category.php?categoryID=2141 [last accessed April 22, 2009].

Waldren, D. and Corrigan, A.F., 1985, An engineering and geological review of the problems encountered in simulating naturally fractured reservoirs. In SPE Middle East Oil Technical Conference and Exhibition, Bahrain, 311-316.

Wang, X., 2005, Stereological Interpretation of Rock Fracture Traces on Borehole Walls and Other Cylindrical Surfaces. PhD Dissertation, Virginia Polytechnic Institute and State University, Blacksburg, Virginia, 113pp.

Warburton, P. M., 1980, A stereological interpretation of joint trace data. Int. J. Rock Mech. Min. Sci. Geomech. Abstr. 17, 181–190.

Zhang, L., Einstein, H.H., and Dershowitz, W.S., 2002, Stereological relationship between trace length and size distribution of elliptical discontinuities, Geotechnique, Vol. 52, No. 6, 419-433.

Tables

Table 1: Fracture intensity data for Tensleep Formation fractures.

# of Fractures	25-1-X-14	48-X-28	61-2-X-15	67-1-X-10	71-1-X-4	Average
Upper Sand	5	5	2	0	7	4
Dolomite	12	8	1	7	0	6
Lower Sand	4	5	3	9	2	5
Total	21	18	6	16	9	14
P10 (m^{-1})	25-1-X-14	48-X-28	61-2-X-15	67-1-X-10	71-1-X-4	Average
Upper Sand	0.178	0.185	0.141	0.000	0.258	0.152
Dolomite	0.628	0.400	0.048	0.355	0.000	0.286
Lower Sand	0.067	0.082	0.049	0.150	0.039	0.078
Average	0.291	0.222	0.080	0.168	0.099	0.172
P32 (m^{-1})	25-1-X-14	48-X-28	61-2-X-15	67-1-X-10	71-1-X-4	Average
Upper Sand	1.994	4.418	0.147	0.000	5.183	2.348
Dolomite	8.564	31.063	0.296	10.369	0.000	10.058
Lower Sand	4.859	3.551	0.192	1.955	0.742	2.260
Average	5.139	13.011	0.212	4.108	1.975	4.889

Table 2: Expressions for determining μ_a and σ_a from μ_l and σ_l.

Distribution for of g(a)	μ_a	$(\sigma_a)^2$
Log-normal	$\frac{128\mu_l^3}{3\pi^3 M\left(\mu_l^2+\sigma_l^2\right)}$	$\frac{1536\pi^2\left(\mu_l^2+\sigma_l^2\right)\mu_l^4-128^2\mu_l^6}{9\pi^6 M^2\left(\mu_l^2+\sigma_l^2\right)^2}$
Negative exponential	$\frac{2\mu_l}{\pi M}$	$\left[\frac{2\mu_l}{\pi M}\right]^2$
Gamma	$\frac{64\mu_l^2-3\pi^2\left(\mu_l^2+\sigma_l^2\right)}{8\pi M\mu_l}$	$\frac{\left[64\mu_l^2-3\pi^2\left(\mu_l^2+\sigma_l^2\right)\right]\left[3\pi^2\left(\mu_l^2+\sigma_l^2\right)-32\mu_l^2\right]}{64\pi^2 M^2\mu_l^2}$

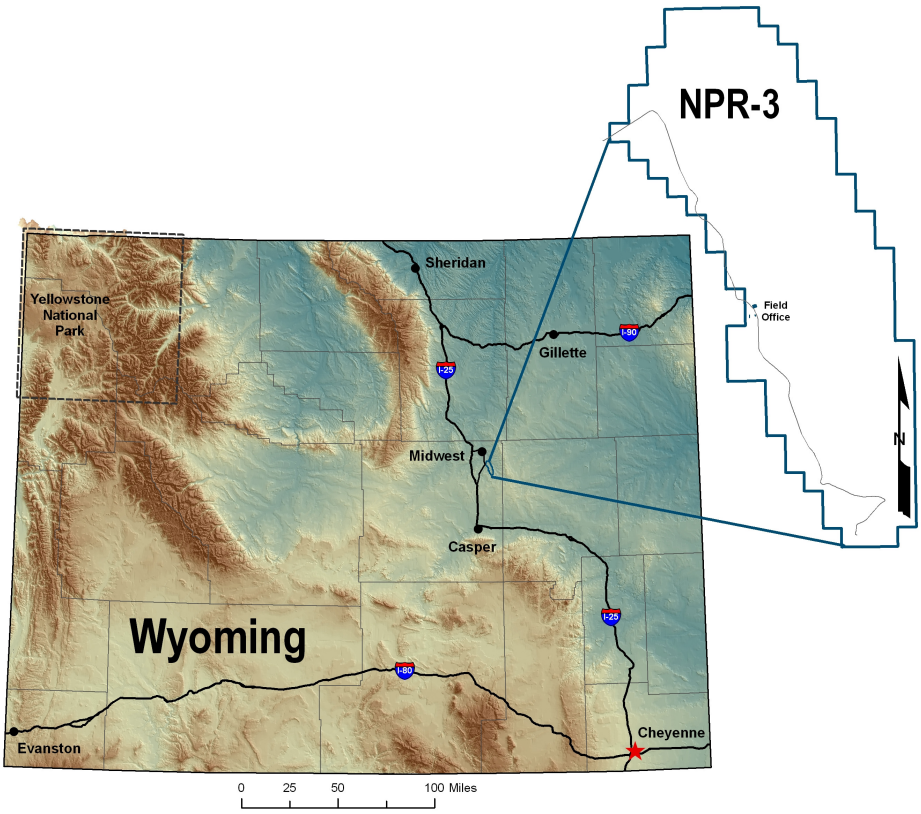

Figure 1: Location of Teapot Dome Oil Field, formerly Naval Petroleum Reserve #3 (NPR-3).

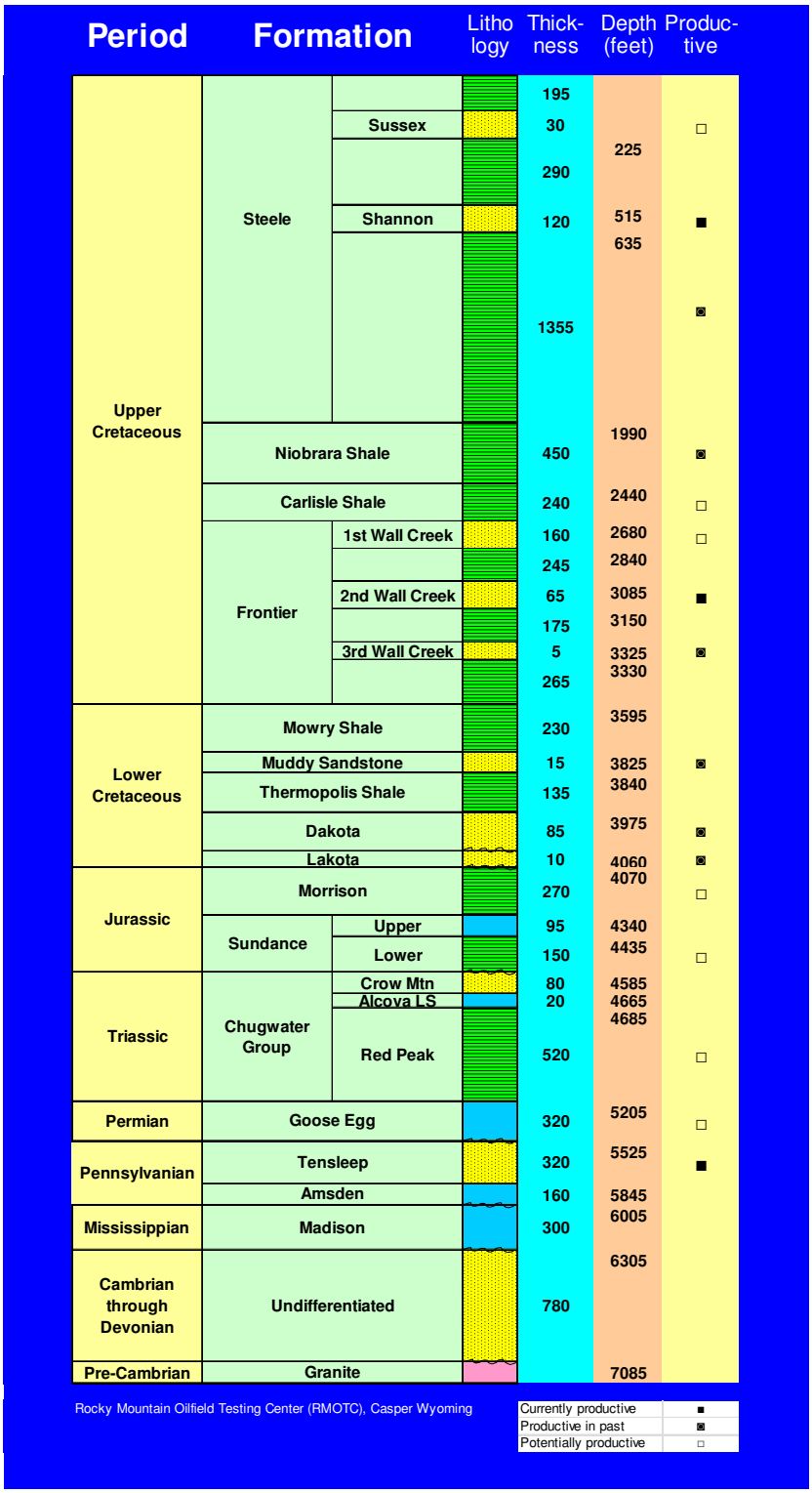

Figure 2: Teapot Dome Geologic Column (from the RMOTC).

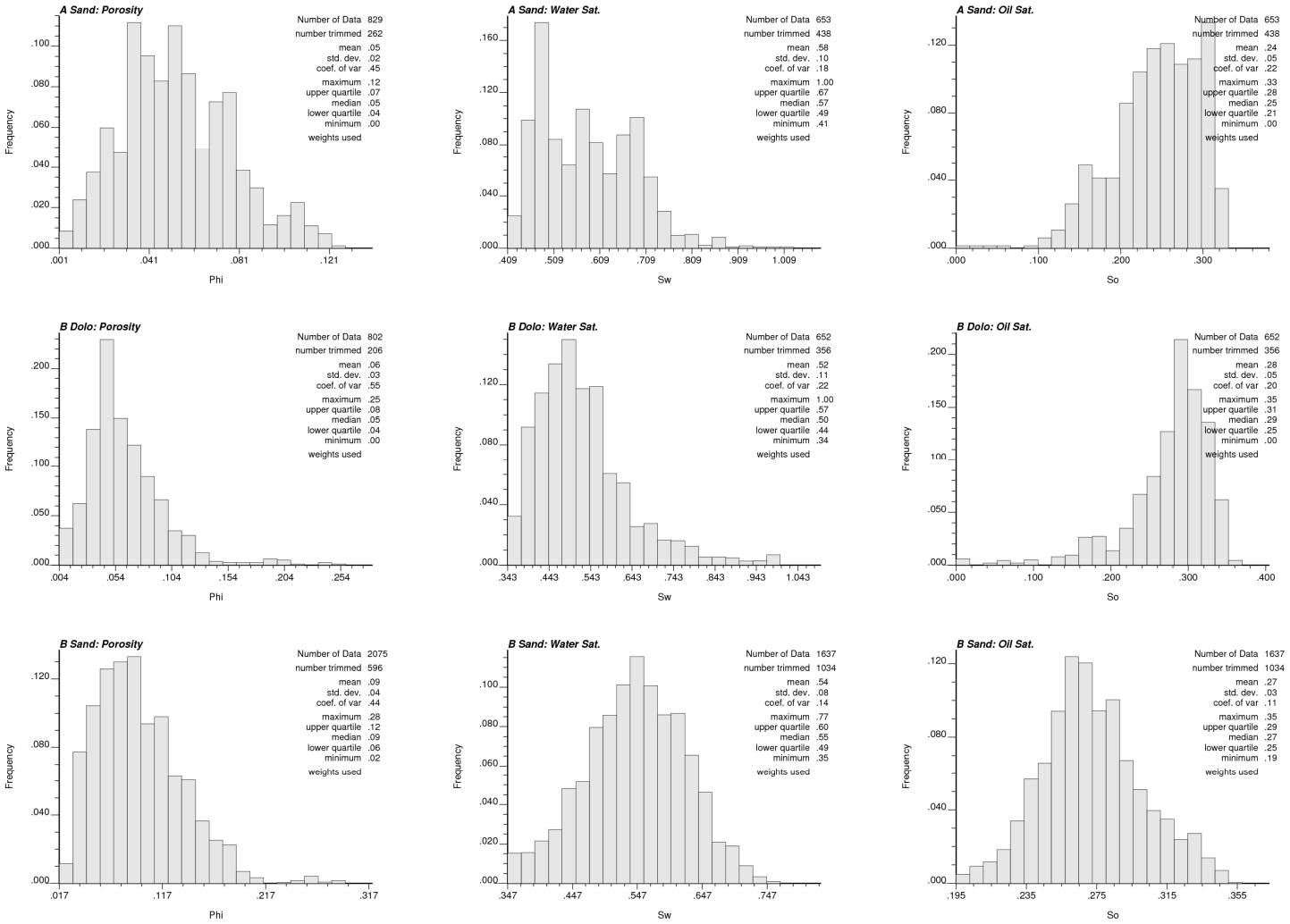

Figure 3: Histograms of porosity, water saturation and oil saturation for the A Sandstone, B Dolomite and B Sandstone units.

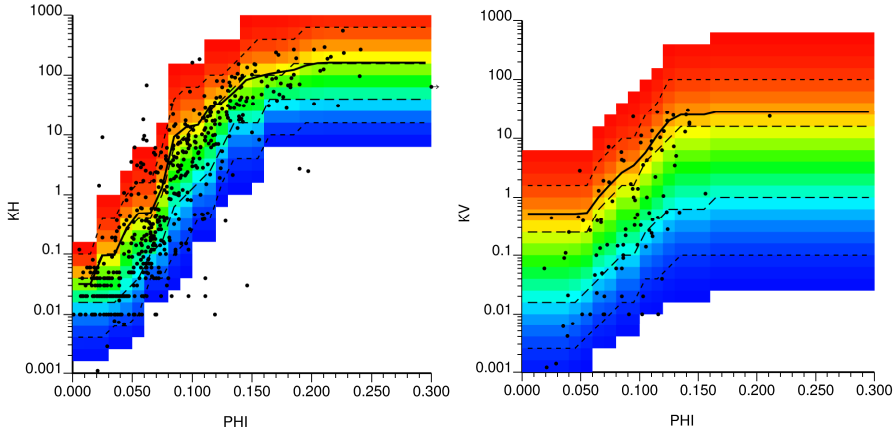

Figure 4: Calculated bivariate relationships between porosity and horizontal and vertical permeability.

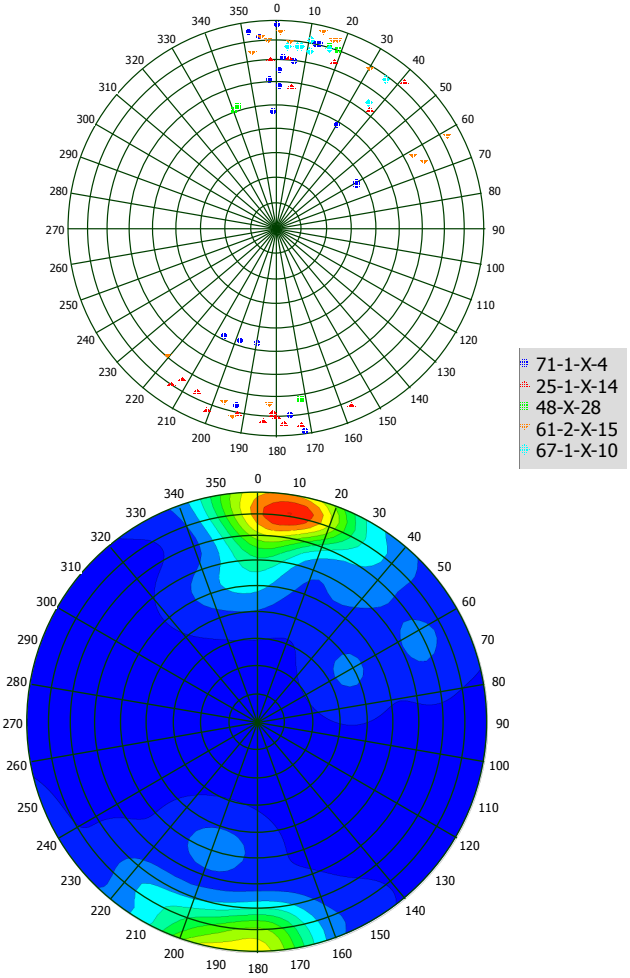

Figure 5: Stereonet of fracture pole orientation and contoured pole orientation.

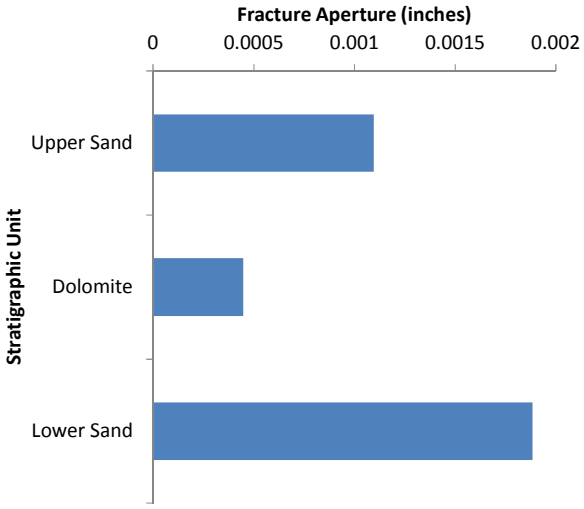

Figure 6: Average fracture aperture by unit.

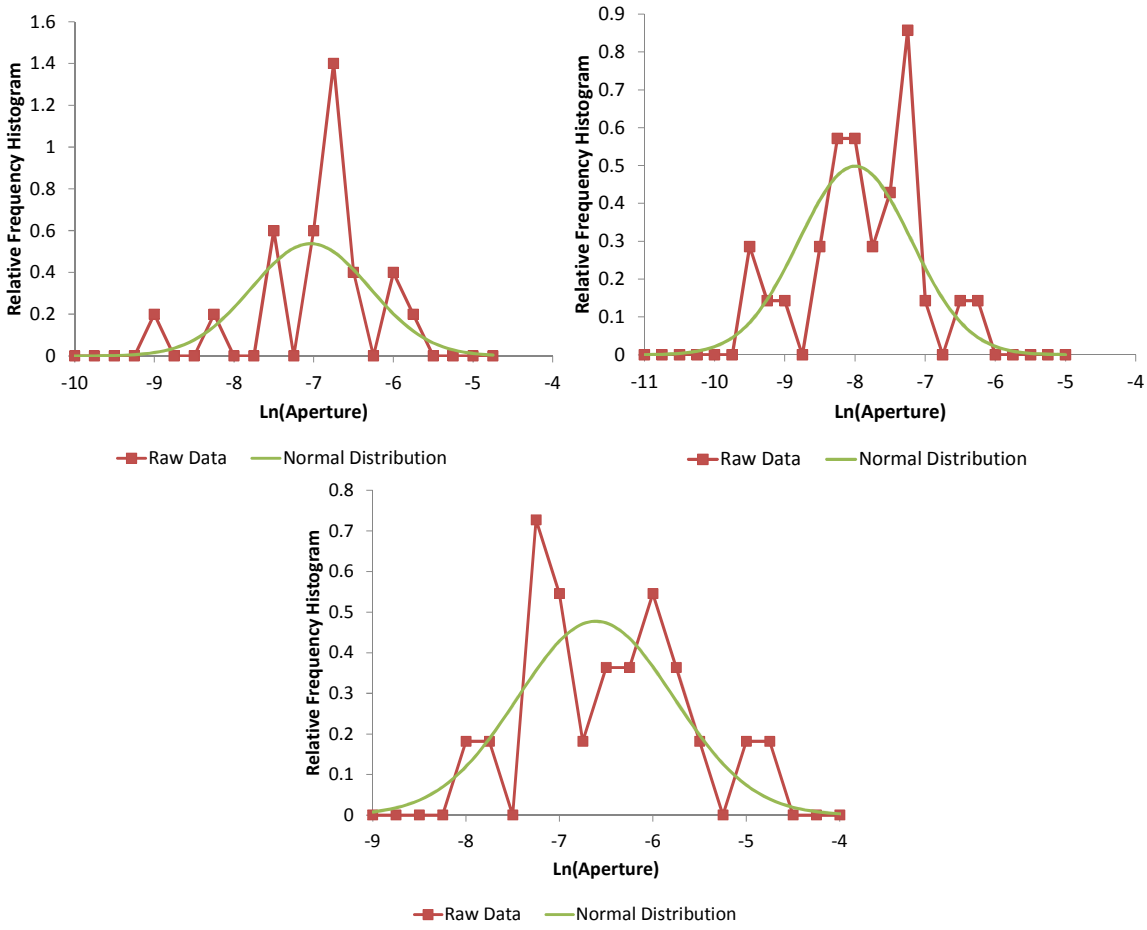

Figure 7: Relative frequency histograms of Ln(aperture) (red line with squares) compared with normal distributions using the mean and standard deviation of Ln(aperture).

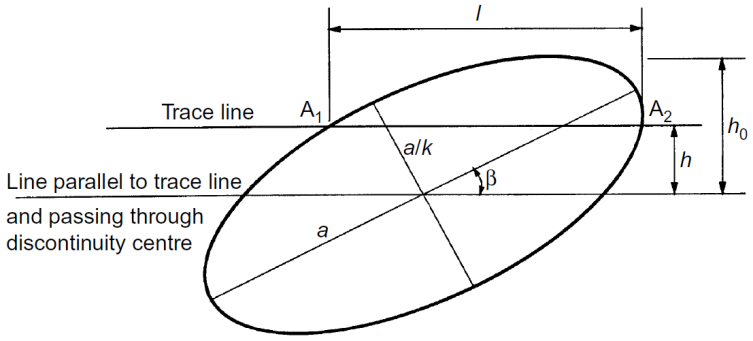

Figure 8: Parameters used in the definition of an elliptical discontinuity (after Zhang, Einstein and Dershowitz, 2002).

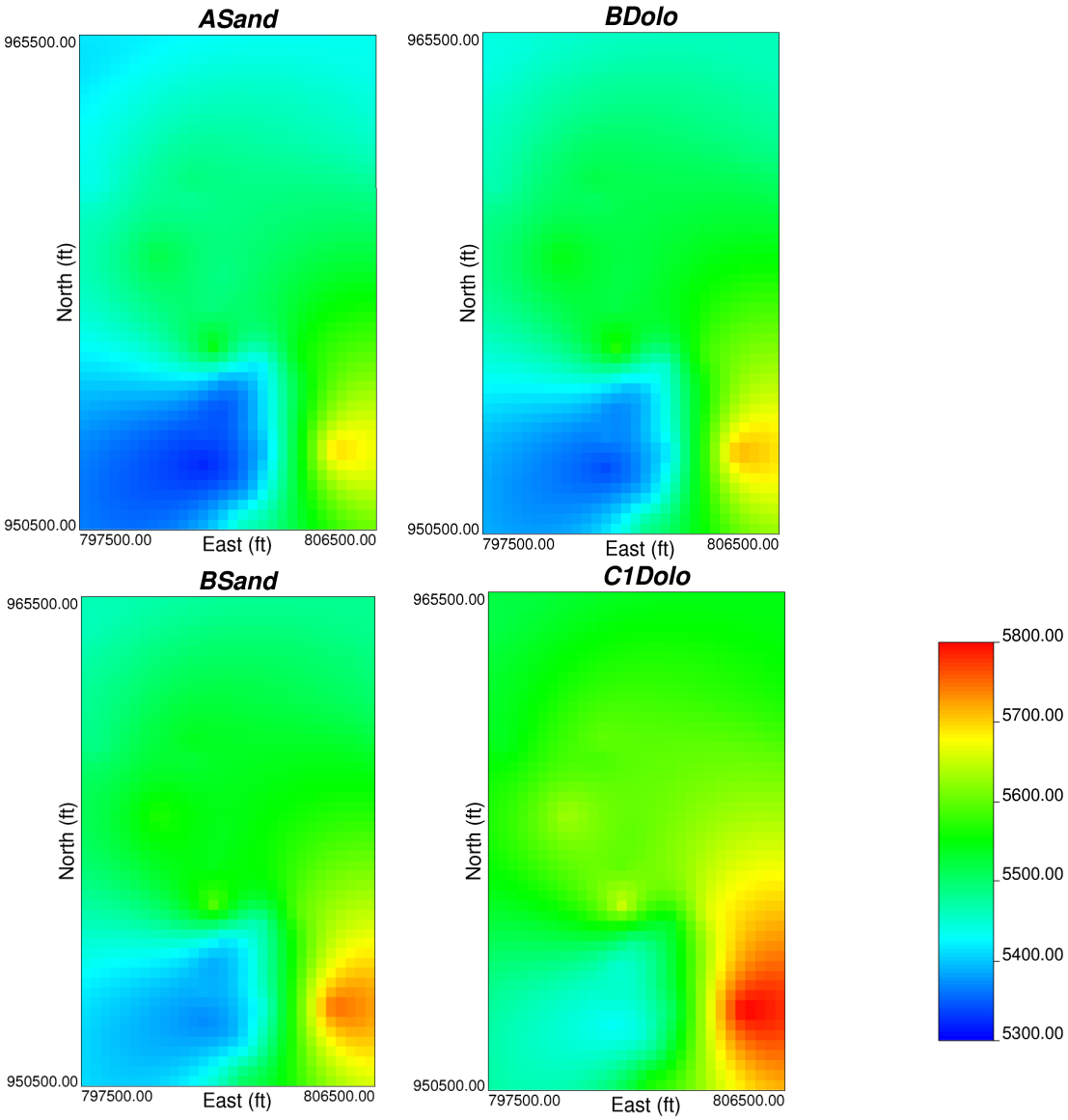

Figure 9: The four kriged stratigraphic surfaces (elevation in feet above sea level).

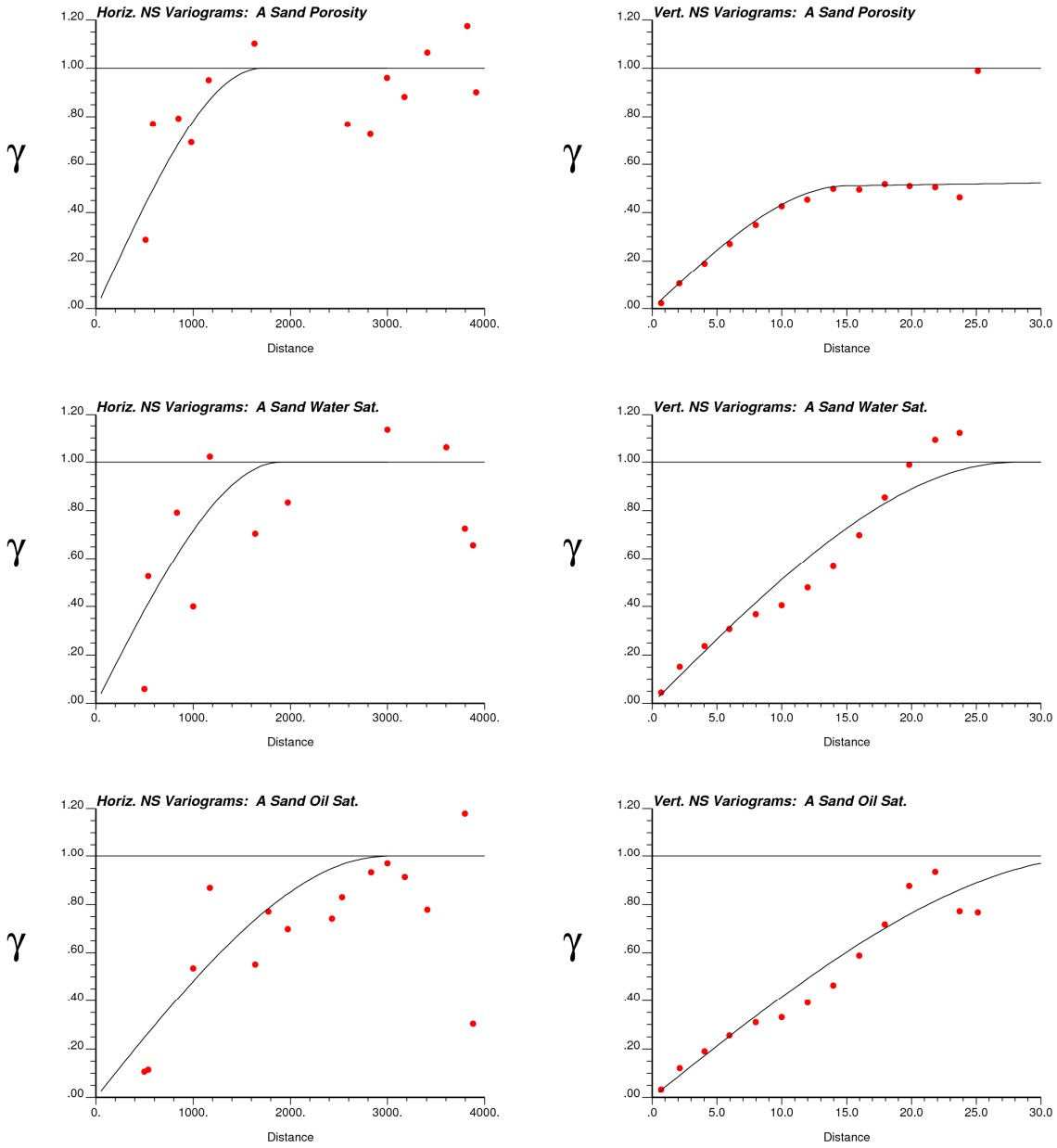

Figure 10: Horizontal and vertical normal score semi-variograms for the A Sandstone Unit (top row = porosity, middle row = water saturation, bottom row = oil saturation).

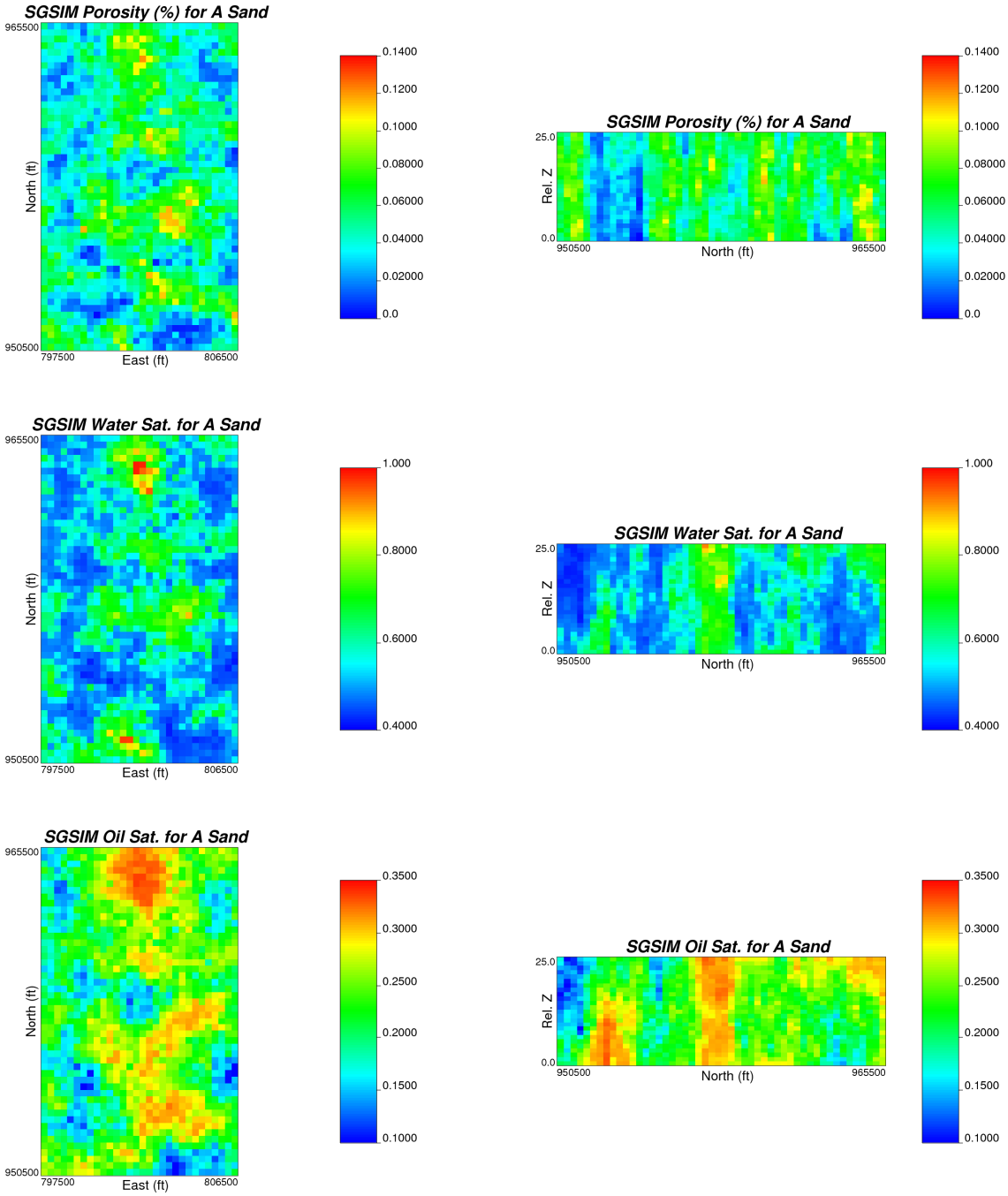

Figure 11: Simulated porosity, water saturation and oil saturation in the A Sandstone.

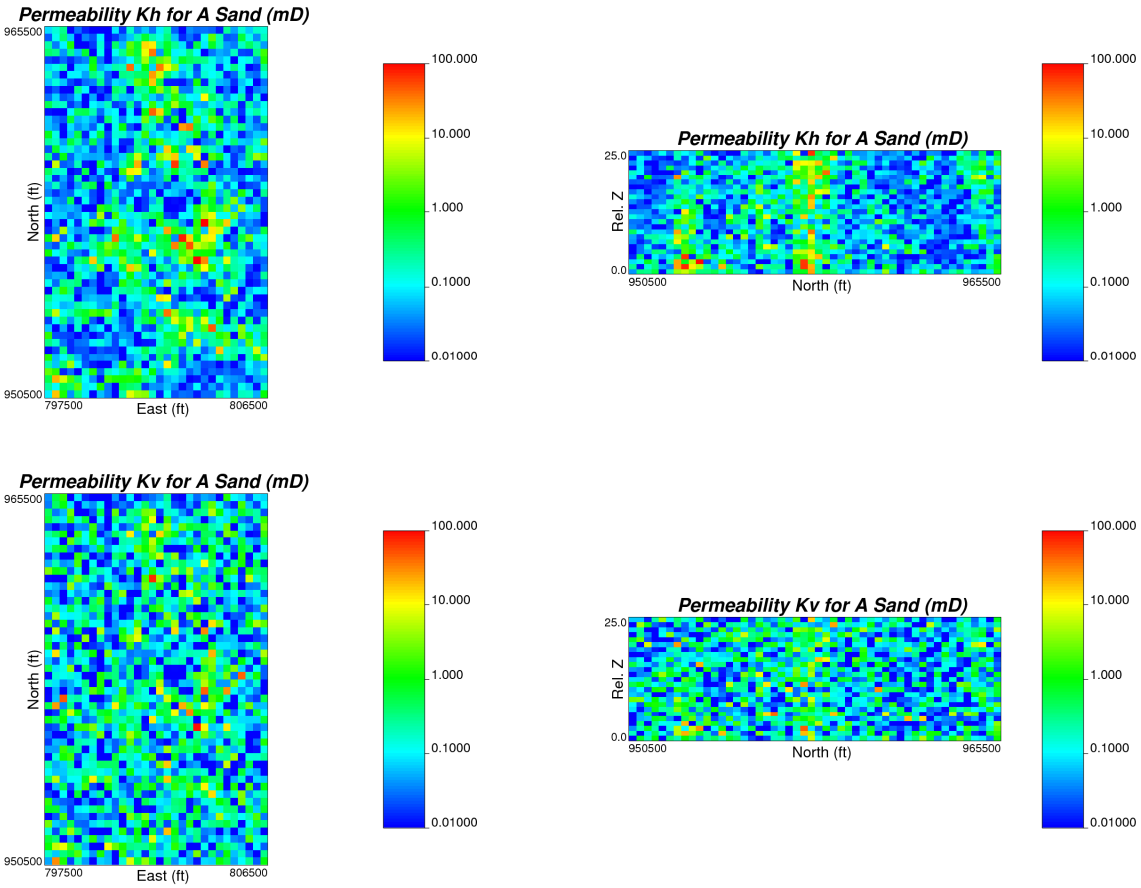

Figure 12: A horizontal and vertical permeability realization in the A Sandstone.

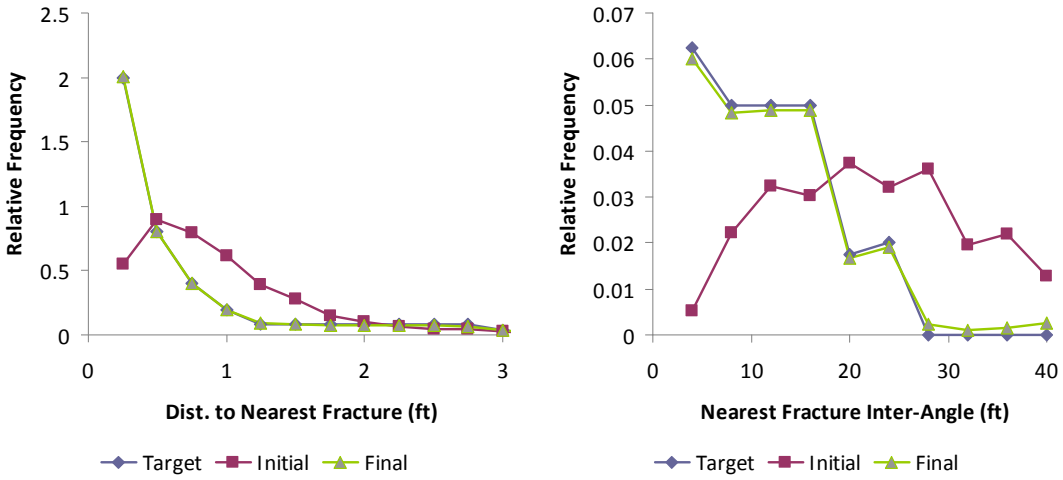

Figure 13: Target, initial DFN and final DFN distributions of local fracture spacing (left) and local fracture orientation.

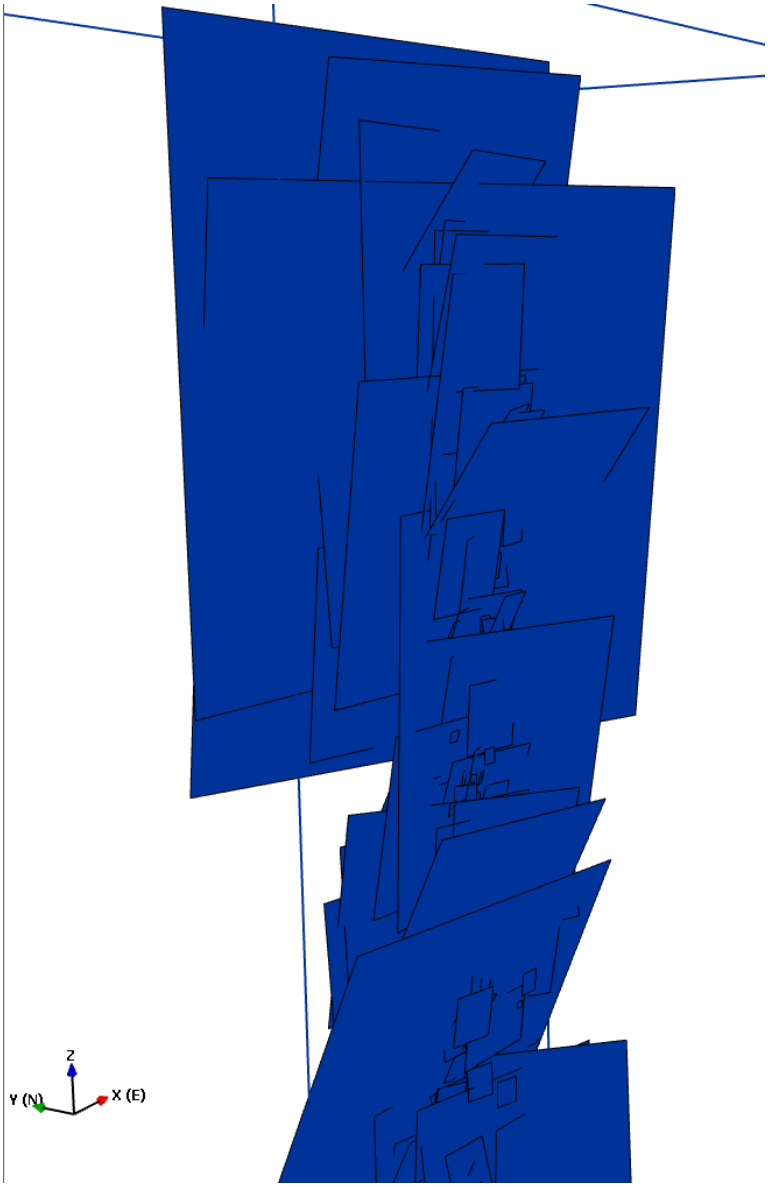

Figure 14: Example discrete fracture network for well 25-1-X-14 in the A Sandstone.

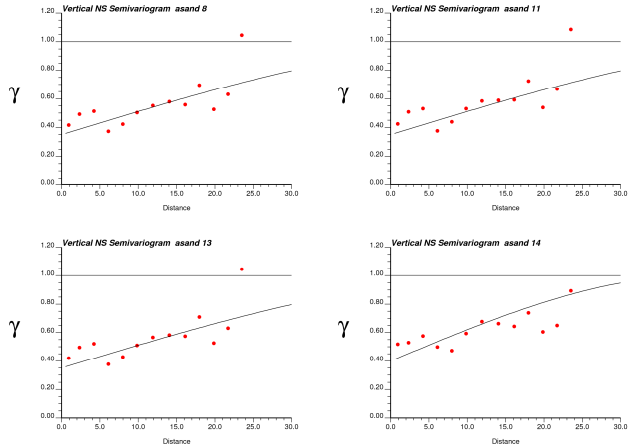

Figure 15: Vertical semi-variograms for Kxx (top left), Kyy (top right), Kzz (bottom left) and fracture porosity (bottom right).

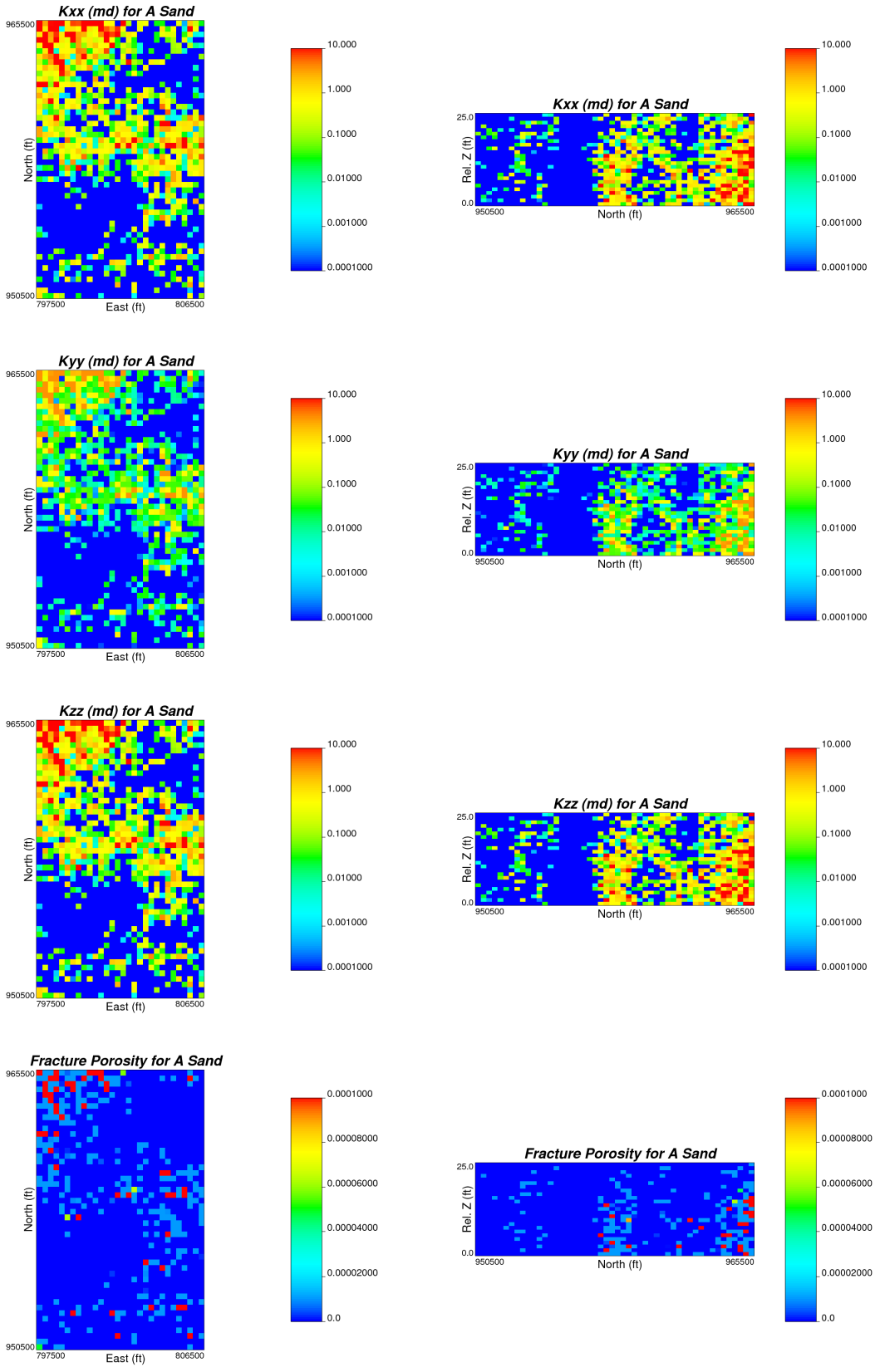

Figure 16: One realization of Kxx, Kyy, Kzz and fracture porosity in the A Sandstone.